A Fiber Optic Probe for Tumor Laser Ablation with Integrated Temperature Measurement Capability

A Fiber Optic Probe for Tumor Laser Ablation with Integrated Temperature Measurement Capability

R. Gassino, Y. Liu, M. Konstantaki, A. Vallan, *Senior Member, IEEE*, S. Pissadakis *Member, OSA* and G. Perrone *Senior Member, OSA, Member, IEEE*

***Abstract*—The paper presents the characterization results of a new all-optical applicator for improved tumor laser ablation treatments that features customized irradiation pattern and built-in temperature sensors. The probe exploits a double cladding optical fiber to integrate some Bragg gratings acting as temperature sensing elements in the core, while guiding the high power beam used for the ablation in the inner cladding. The assessment of the probe behavior has been conducted in two steps: first, with an agar gel phantom to characterize the irradiation pattern and to validate the Bragg grating based measurement setup in comparison with a thermographic camera; then, simulating actual treatments using an ex-vivo animal liver.**

***Index Terms*—Tumor laser ablation, Hyperthermal treatments, Fiber Optical Sensors, Fiber Bragg Gratings, Temperature measurement**

I. Introduction

MINIMALLY invasive treatments of solid tumors based on electromagnetic waves - the so-called thermo-therapies or ablations - are attracting an increasing interest because they can constitute an effective alternative to surgical resection, not only with lower physical impact, but also capable of a substantial reduction in the overall intervention costs [1]–[3]. Depending on the frequency of the electromagnetic waves, thermal ablation is generally classified into Radio-Frequency Ablation (RFA), MicroWave Ablation (MWA) and Laser Ablation (LA), also known as Laser-Induced Thermo-Therapy (LITT). Regardless of the specific operating principle, malignant cells are killed by raising the tumor mass temperature slightly above cytotoxic level (e.g., higher than about $50\,^{\circ}\mathrm{C}$ to $60\,^{\circ}\mathrm{C}$ [1], [2], [4]) trough specific applicators; for deep lying organs the applicators are inserted percutaneously using capillary needles guided to the right position with the help of Ultra-Sonic (US), Magnetic Resonance (MR) or Computed Tomography (CT) imaging [5].

LA is the most recent of these thermal treatments and, although still not largely employed as routine clinical technique, it has already shown great potential for becoming the elective thermo-therapy for a broad range of carcinomas, such as those in the liver, pancreas, kidneys and thyroid, to name the most relevant [3], [6]–[8]. LA uses optical fiber-based applicators to guide the laser beam into the tumor mass and cell death is induced through the heat generated by light absorption; besides for the advantages intrinsic to the laser-based treatment, by making use of all-dielectric applicators it is the only ablation approach fully compatible with MR Imaging (MRI). There are, however, limitations in LA too, mainly related to the control of the laser energy effect, such as the lack of control on the laser irradiation pattern and of real-time feedbacks about the therapy outcome. In particular, it has been shown that an improvement in the therapy effectiveness can be obtained by careful monitoring of the ablation process parameters, the most important being the induced temperature increase [2]. Indeed, while the temperature of the target area should be raised to cytotoxic values, excessive water evaporation and tissue carbonization must be avoided. Control of temperature translates for LA mainly into control of laser power and exposure time. The laser absorption, however, depends on many factors so a priori temperature predictions are difficult and not always accurate enough. Actual temperature increase can be measured with many approaches, the most common being the use of thermocouples or of thermistors, as done in other forms of thermal ablation such as RFA. However, these components are not easy to integrate into fiber-based probes and, moreover, being metallic, they interact with the laser beam and introduce measurement artifacts. As an alternative, the already mentioned imaging techniques (US, MR and CT)) can provide temperature variation estimations in near-real time too, but, due to equipment availability, operation complexity and other limitations specific of each of these technique, they are difficult to be used as routine methods [9], [10]. Another possibility is to use fiber optic sensors since they can be made transparent to the high power ablation beam and have a reduced footprint, so they do not introduce localized overheating or other relevant heat distribution perturbations. Particularly interesting are the sensors based on Fiber Bragg Gratings (FBGs) [13] because already extensively investigated as temperature sensors both in biomedical [14] [15] and non-biomedical [16] [17] applications; moreover they are able to measure temperatures with uncertainty below $1\,^{\circ}\mathrm{C}$ [18], exhibit good stability [19] and have reduced dimensions [20]. Temperature measurement requirements can be indeed rather demanding, as accuracy better than few degrees, with spatial resolution better than $1\,\mathrm{cm}$ and time response below $1\,\mathrm{s}$ are typically requested to precisely monitor the temperature distribution over the area under ablation, especially during the fast tissue heating phase [11], [12].

To help overcoming some of the previously outlined limitations in LA, we have developed a probe that integrates a

R. Gassino, Y. Liu, A. Vallan, and G. Perrone are with the Dipartimento di Elettronica e Telecomunicazioni, Politecnico di Torino, corso Duca degli Abruzzi, 24 - 10129 Torino (Italy); e–mail: alberto.vallan@polito.it, guido.perrone@polito.it

M. Konstantaki, and S. Pissadakis are with the Institute of Electronic Structure and Laser, Foundation for Research and Technology - Hellas, N. Plastira 100, Heraklion 70013, Greece e–mail: pissas@iesl.forth.gr

customized laser irradiation pattern with all-fiber temperature measurement capabilities, so it becomes possible matching different tumor shapes and simultaneously monitoring the treatment progress in real-time. In an early work [21] the probe was made by integrating a FBG into the core of a Double Clad Fiber (DCF). DCFs are specialty fibers with a three layer structure (core, inner cladding, outer cladding) commonly used for high power fiber amplifiers and lasers [22]: for these applications the core is used to guide the laser signal, whereas the inner cladding the pump power; in our application, the core is used to guide the temperature sensing signal, and the inner cladding the high power beam used for ablation. This probe had the limitation of having a single temperature measurement point, moreover averaged over the entire grating length (1 cm to 2 cm), which can be non negligible in many practical cases. In a more recent work [23] we developed an applicator with multi-point all-optical temperature sensing capabilities by surrounding a high power large area delivery fiber with a set of standard single-mode fibers with FBGs inscribed in their cores. These sensing fibers were scaled along the longitudinal direction to improve the spatial resolution despite the length of the gratings. Nevertheless the use of uniform FBGs limit the spatial temperature measurement resolution, so alternative techniques have been sought. Some studies are aimed at the use of Chirped FBGs (CFBGs), while others exploit the Optical Frequency Domain Reflectometry (OFDR). CFBGs are characterized by a variable period of the refractive index perturbation, so that different wavelengths are reflected at different points along the grating length; this way, it is in principle possible to relate the shape of the grating spectral response with the temperature profile distribution: the technique is promising, although it cannot be considered reliable for practical clinical applications yet [24], [25]. OFDR exploits the changes in the amplitude, frequency and phase of continuously back-scattered Raman, Brillouin or Rayleigh light along the fiber to recover temperature and deformation profiles over lengths that can extend up to several kilometers [26]. It is a very powerful approach that has been so far mainly applied to civil structural monitoring (e.g. pipelines, bridges, etc.); with respect to the application targeted in this paper, these systems are able to provide accurate enough temperature resolution (down to $0.1\,^{\circ}$C), but usually fails in terms of spatial resolution (order the meters) or integration time (order of hundreds of seconds) [27], [28], with the exception of an OFDR method based on coherent demodulation of Rayleigh backscattering [29]. The commercial implementation of the latter has been used to evaluate the temperature profile distribution during simulated RFA procedures using liver phantoms [15]: the results are very promising and the same approach could be applied for LA as well. However, in the cited paper the induced temperature increase has been measured though a stand-alone fiber and further investigations would be necessary to evaluate the impact of possible perturbation effects due to the high power laser beam when a DCF structure is used to integrated both delivery and sensing fibers, as in the probe considered in this paper. Moreover, highest resolution is achieved only with the help of post-processing routines, making real-time accurate evaluations almost impossible.

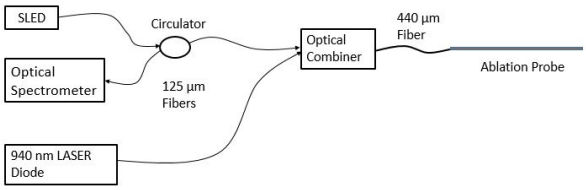

Fig. 1. Layout of the laser ablation system with integrated temperature measurement capability.

Therefore, in view of clinical tests, which typically require more consolidated approaches, in this paper we present an improved version of the LA applicator that integrates in the core of a DCF a plurality of temperature sensing gratings and we report on the characterizations aimed at evaluating through their readings the extension of the ablated area. The remaining of the paper is organized as follows. Sect. II presents the development of the laser ablation system and the realization of the probe, while Sect. III describes the probe characterization using an agar gel phantom to mimic working conditions similar to those found when treating liver tumors but without reproducibility issues. Then, Sect. IV discusses the results obtained in laser ablation simulations using an ex-vivo animal liver and Sect. V draws the conclusions.

II. Laser Ablation System Development

The laser ablation system layout in sketched in Fig. 1 and is composed of a few watt laser source, a home-made FBG interrogation system, an ad-hoc combiner to multiplex the high power beam with the sensing signal, and a probe with customized irradiation pattern combined with all-optical temperature sensing capability.

The high-power laser source is a diode module able to deliver up to 10 W at 915 nm (nominal value, but any diode in the 9xx nm range would fit), a wavelength chosen because of the good balancing between tissue absorption and penetration depth [30], [31] and for the reasonable cost-per-watt being these modules largely employed for pumping high power fiber lasers [22]. The FBG interrogator is made by a Super-luminescent Light Emitting Diode (SLED) coupled to a handheld spectrometer through a circulator and allows estimating the temperature changes in different locations by measuring the shift of the peak positions in the spectrum reflected by wavelength multiplexed FBGs acting as temperature transducers. Since the resolution provided by the spectrometer is about 100 pm, which is too coarse to meet the application requirements, specific signal processing real-time routines are used to improve it, down to few picometers, corresponding to approximately 0.2° to 0.5° depending on the grating spectrum profile and working conditions [12]. As already mentioned, the probe is made out of a dual cladding fiber, similar to those of high power fiber lasers [22], but in which the inner cladding is used to guide the laser ablation beam and the core the sensing signal (Fig. 2). In our applications we tested different fibres with core ranging from 10 µm to 20 µm, inner cladding diameter ranging from 200 µm to 600 µm and outer cladding

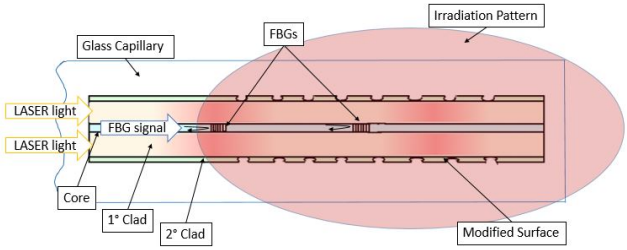

Fig. 2. Schematic representation of the all-fiber probe based on a dual cladding fiber.

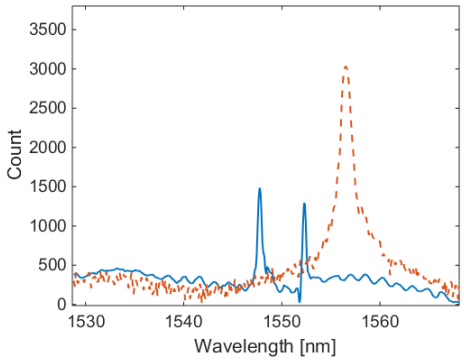

Fig. 3. Reflection spectra of some of the fiber Bragg gratings used as temperature sensors in the experiments reported in this paper: two gratings inscribed in core of a 20/400 dual-clad fiber (blue) and one of gratings used as stand-alone sensors external to the probe for characterization purposes (red).

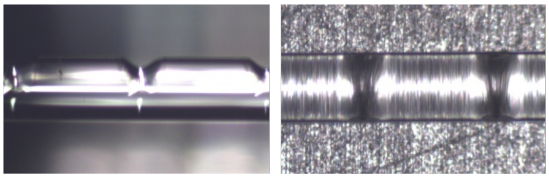

Fig. 4. Picture reporting the detail of the local perturbations of the fiber surface acting as irradiation points: side (left) and top (right) views.

some 200 µm larger than the corresponding inner cladding. No appreciable changes in the optical performance have been recorded, so the fiber diameter can be chosen according to mechanical requirements only, in particular considering the diameter of the catheter through which the applicator will be inserted. In practice, a quite large inner cladding diameter of 400 µm is likely to be used for most of the applications as a compromise between invasive impact and mechanical robustness.

The fiber Bragg grating acting as temperature sensors are inscribed into the fiber core by using a standard phase mask setup and a 193 nm high coherence excimer laser source that delivers 190 mJ/cm^2 energy density with 10 ns pulses and 30 Hz repetition. Fig. 3 reports the reflection spectra of two of these gratings inscribed in the core of a 20/400 DCF, together with the spectrum of another grating inscribed in a common single-mode fiber, which has been used as an additional temperature sensor to be placed outside the applicator for comparisons. To inscribe two consecutive Bragg gratings in the same core, first the fiber is irradiated through a phase mask having a first period (e.g., 1073.20 nm for one of the gratings whose spectrum is shown in Fig. 3), then it is translated by 8 mm and exposed again through a mask having a second period (e.g., 1070 nm for the other of the gratings whose spectrum is shown in Fig. 3). For example, the inscription whose results are reported in Fig. 3 resulted in two well defined Bragg reflection peaks with spectral separation of 4.5 nm. Having more than one grating in the fiber core allows quasi-distributed temperature measurements and thus a better evaluation of the induced temperature profile, especially to overcome possible underestimations when one of the gratings happens to be positioned close to a blood vessel. FBGs, however, have also the drawback of a relevant cross-sensitivity with strain. This aspect has been effectively exploited in some applications [32], but here it represents a serious drawback since strain effects can not be distinguished from temperature effects. To help mitigating this problem, we protected the sensitized portion of the fiber by inserting it into a quartz capillary, which is then collapsed on one end to seal it; we verified that this solution is effective and introduces negligible optical perturbations and acceptable thermal inertia contributions [12].

Finally, customized irradiation patterns to match specific tumor sizes and shapes are obtained through beam diffusers fabricated by laser assisted micro-patterning of the fiber tip surface after having removed the outer cladding [23]. A 100 W CO_2 laser set at approximately 10% power output is used to induce on the fiber surface local damages that will act as irradiation points. If irradiation is required all around the fiber (as for example when the applicator is inserted in the middle of the tumor mass), the process has to be repeated after having properly rotated the fiber. In a preliminary development phase we had related the power and the scanning speed of the laser beam with the depth of the induced damage and thus with the desired local irradiation intensity to allow producing customized patterns [21]; nevertheless, to have a better control of the results, the irradiation pattern due to the induced fiber surface modifications is continuously monitored after each scan of the CO_2 laser by feeding the fiber with the high power laser beam and recording the irradiation image through a camera. An example of the obtained surface modification is shown in Fig. 4.

The probe irradiation pattern and temperature sensor position should be optimized depending of the tumor shape and size; however, since the scope of the paper is not to present a specific application but the probe structure itself and describe its characterization, a probe with an almost uniform irradiation has been used for the reported examples. This has been fabricated by repeating the surface micro pattern three times after having rotated the fiber by 120°. Then, the lateral irradiation characteristics affect also the residual power that is radiated through the end face: in the considered probe this is approximately 10%.

The peculiar use of the DCF requires the development of a special fused fiber combiner ("Optical combiner" in Fig. 1)

to properly route sensing and ablating signals. This is realized using a tailored version of the devices known as $(N+1) \times 1$ "pump combiners with feed-through fiber" typically used in high power fiber laser applications [22].

III. Temperature Measurement Assessment

A. Measurement Setup

The probe capability to create a wide enough area having the temperature values required for an effective laser ablation and to provide adequate feedback to the operator about the obtained temperature has been assessed using the setup depicted in Fig. 5 with the following procedure.

1) Realization of a phantom to simulate typical working conditions, but in a more controlled environment (avoidance of tissue variability and temperature profile distorting agents, like blood vessels).
2) Validation of the grating sensors using a particular configuration of the phantom that allows comparing the temperature read in different locations by the FBGs with that obtained with a thermographic camera.
3) Simulation of an actual laser ablation procedure (a condition that does not allow using a thermographic camera) and estimation of the effectiveness of the treatment relying for the temperature measurement on the reading of the gratings only.

Targeting the ablation of deep-laying organs, we chose for the phantom material an ink-loaded agar gel with suitable composition to mimic optical and thermal properties of liver [23], [30], [33], [34]. Then, to easily insert the probe under test and possibly other additional sensors while maintaining the desired relative positions among them, we cast the gel in the form of two disks that can be superimposed one on the top of the other. This configuration has also the advantage of allowing the thermographic camera to measure the temperature in the same location of the gratings when the upper disk is removed. Of course, the condition that best matches an actual ablation treatment is with the upper disk present, when the temperature distribution at the grating level cannot be measured through the thermographic camera. Therefore, while the temperature along the probe axis can be measured by the integrated gratings, the evaluation of the area affected by the treatment through the measure of the temperature spatial distribution perpendicular to the probe axis requires some additional FBG-based sensors deployed outside the probe, as it can be seen in Fig. 6. Here it is shown an example of a probe with two integrated gratings (FBG4 and FBG5) positioned on the top of the lower agar gel disk together with three additional FBGs used to measure the temperature immediately close to the applicator (FBG1) and at a distance of $0.5\,\text{cm}$ (FBG2) and of $1\,\text{cm}$ (FBG3) from it, respectively. Particular care has to used in laying the FBGs external to the probe to avoid parasitic strains.

Prior to the probe assessment tests, all the FBG-based sensors have undergone extensive characterizations using an environmental chamber and a calibrated thermometer to compute the individual wavelength-shift-to-temperature conversion coefficient.

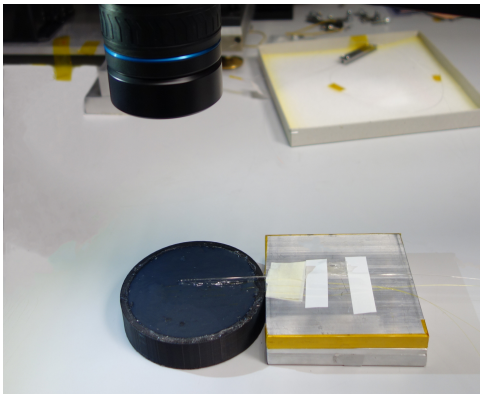

Fig. 5. Picture of probe characterization setup. Fibers lie on the lower agar gel disk and are maintained in the right position using a home-made holder. The temperature distribution on the grating plane is monitored using also a thermographic camera. The upper agar gel disk is not shown in this picture being this the configuration used to compare the readings from the gratings with those from the thermographic camera.

Fig. 6. Close-up of picture in Fig. 5 highlighting one of the developed laser ablation probes together with three other external fiber Bragg grating sensors laid on one of the disks forming the agar phantom.

B. Grating Temperature Sensors Characterization Results

Using the approach outlined in Sect. II, two $5\,\text{mm}$ long Bragg gratings separated by about $3\,\text{mm}$ have been inscribed [35] in the core of some 20/400 DCFs, whose surface has then been modified using a CO_2 laser to produce a uniform radiation pattern that allows treating an area of approximately $3\,\text{cm}$ by $2\,\text{cm}$. In particular, for the probe whose characterization measurements are reported in this paper, both integrated gratings are within the region of almost uniform irradiation. The probes have then been characterized both in terms of laser irradiation pattern and of temperature measurement capabilities using the agar gel phantom and setup previously described.

Fig. 7 shows a comparison among the readings of the gratings positioned as in Fig. 6 during a simulated ablation process. The probes and the additional external gratings are sandwiched between two $3\,\text{cm}$ thick agar gel disks. The laser power was limited to $2\,\text{W}$ to maintain the maximum temperature lower than $50\,^{\circ}\text{C}$ because we experimentally verified a degradation in the agar gel properties above this value. All the gratings have the same time constant, which is mainly due to the agar thermal properties, while the maximum peak shift in their response - thus the temperature read - depends on the grating position with respect to the high power beam delivery. The sensors integrated within the probe (FBG4 and FBG5) and that immediately external in same intermediate

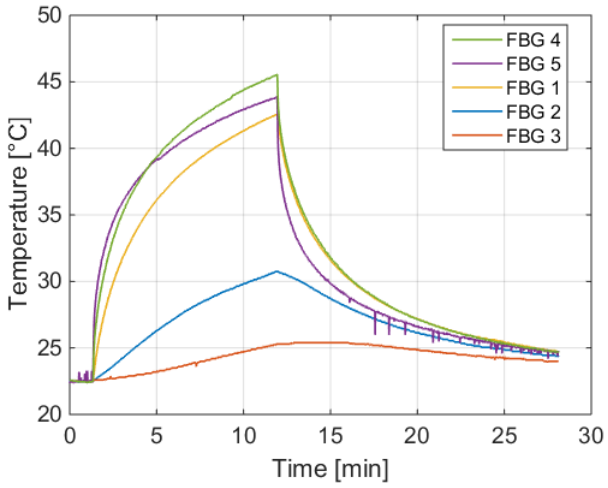

Fig. 7. Comparison among the readings of the various gratings during a simulated ablation process. The laser has been switched off before the maximum temperature reached 50 °C to avoid degradations in the agar gel.

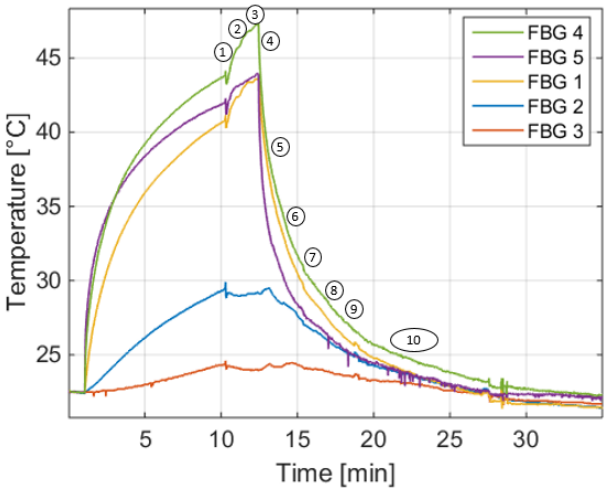

Fig. 8. Temperature read by the various grating sensors during a simulated laser ablation experiment in which at a certain point the upper disk of the phantom is removed; numbers refer to the thermographic images in Fig. 9.

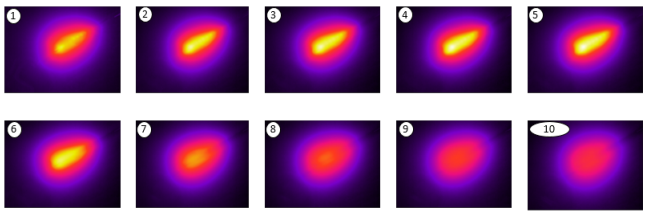

Fig. 9. Thermographic images corresponding to the different time instants numbered in Fig. 8.

position along the irradiation pattern (FBG1) are in good agreement, with maximum temperature difference less than 3 °C. This difference is due to the thermal resistances of the delivery-capillary-agar path. The temperature variation along the transverse direction is about 14 °C between FBG1 and FBG2 (i.e., in about 0.5 cm), and reduces to about 10 °C between FBG2 and FBG3 (i.e., again in about 0.5 cm), denoting a quite large temperature gradient, especially close to the probe. As for probe longitudinal direction, the temperature distribution is quite uniform (the variation between FBG4 and FBG5 is less than 2 °C in about 1 cm), as required for the targeted applications.

To validate the readings of the grating-based sensors we have to make the thermographic camera measure the same temperature distribution and this can be obtained only by removing the upper gel disk. Therefore, in another simulated ablation process we maintained the laser on (again 2 W for allowed maximum temperature reasons) until the temperature reached an almost stable value, then we removed the upper disk, leaving the laser on until temperatures reached about 50 °C. The temperature read by the various gratings during this test are shown in Fig. 8. The curves show a temperature increase in correspondence of the upper disk removal (identified by the small glitch) that is due to the lower conductivity of air with respect to that of the agar. Fig. 9 reports the thermal images taken at the different time instants numbered in Fig. 8: from this set of images it is evident that the laser irradiation pattern is effective in creating a high temperature region around the applicator and that the temperature distribution exhibits a large gradient while the laser is on. This can be graphically appreciated also from Fig. 10, which reports the contour plot of the temperature distribution in correspondence of the first (laser on, therefore ablation in progress) and fifth (close to laser switch-off time) time instants marked in Fig. 8. The isothermal lines defining the area with cytotoxic temperature values when the laser is on has an elliptical shape as expected, with eccentricity of about 0.9, which is close to the target value.

Thermal images and grating results are in good agreement as it can be seen from Fig. 11 that compares the readings from the thermographic camera and those of the external FBG1, FBG2 and FBG3 gratings added for profile characterization purposes. The curves corresponding to the integrated gratings FBG4 and FBG5 have been omitted for clarity; nevertheless the correspondence between the reading from the gratings inscribed inside the probe and FBG1 has already been proved in Fig. 8). During normal operation (i.e., when the laser is on) the maximum error is limited to less than 0.7 °C and this validates the readings from the external gratings and thus their

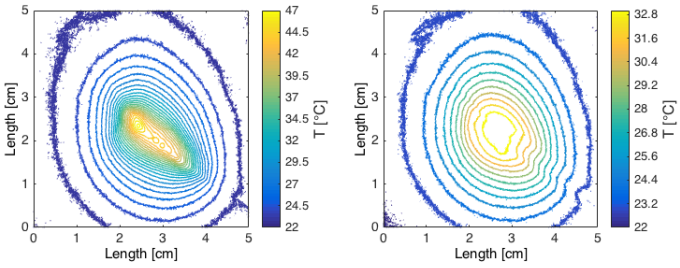

Fig. 10. Contour plots of the temperature distribution in correspondence of the first and fifth time instants in Fig. 8. The leftmost plot is for a laser on conditions and allows determining the area where ablation if effective because corresponding to a cytotoxic temperature value (yellow curves).

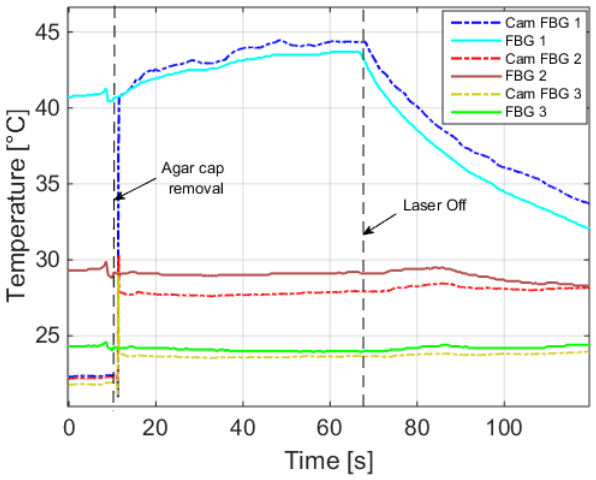

Fig. 11. Detail of Fig. 8 around the time at which the upper disk is removed and comparison of with corresponding temperature read by the thermographic camera.

use to estimate the area where ablation takes place.

IV. Example of Applications

The tests with the agar phantom have been used to validate the correspondence between the readings of the thermographic camera and those of the FBG-based temperature sensors, both integrated within the probe and added externally for characterization purposes. Actual evaluation of the probe behavior, however, requires a more realistic phantom, since, for instance, in practical cases light absorption is strongly dependent on the local tissue composition. This has been done reproducing with an ex-vivo animal liver the same setup as that used with the agar phantom (Fig. 12): we cut the liver in two slices to allow "sandwiching" the applicator and the other sensors used for its characterization while precisely controlling their relative positions. In actual applications, in which only the applicator will be necessary, this will be inserted in the organ through a metallic catheter of suitable diameter (these catheters are common in surgical interventions and exists in many size, expressed in french scale [36]) that will then be retracted to expose the applicator and allow it freely radiate. Since the external FBG1, which is in strict contact with the laser probe, had already been demonstrated to be in good agreement with the inscribed FBG4 and FBG5, to simplify the layout in the setup shown in Fig. 12 we omitted this external grating. As for FBG2 and FBG3, they have been placed in about the same position as in the agar phantom.

As reported in Tab. I, different tests have been carried out keeping the energy constant, but with power ranging from 2 W to 4 W. As general comment, in all the cases the duration of the ablation is shorter than that with the gel phantom because a faster stabilization of the temperature has been observed. This also highlights the importance of non limiting the characterization of the probes to the use of gel phantoms only; this has been important as a preliminary step to validate the reading the grating-based sensors in comparison with those of a thermographic camera or to image the irradiation pattern

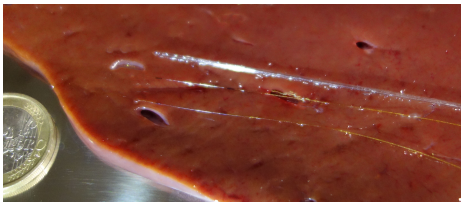

Fig. 12. Photo of the probe with two external gratings used to evaluate the irradiated area before the beginning of the liver ablation procedures. The 1 Euro coins allows a immediate visual estimation of the sizes.

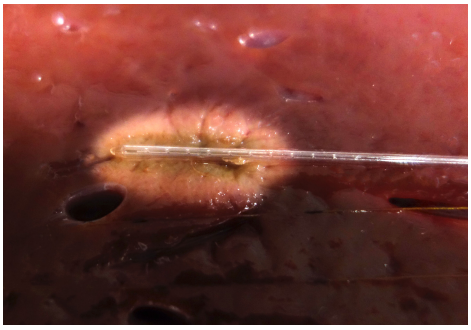

Fig. 13. Picture of the ablation obtained with 2 W of power for 150 s.

in conditions as close as possible to those found in practical uses, but the actual behavior of the probe can be evaluated only using a real liver, albeit ex-vivo.

TABLE I
Summary of the tests carried out using the ex-vivo liver.

Power [W]	2	2	3	4
Energy [J]	300	300	300	300
FBG2 [°C]	50.4	57.3	37.9	58.7
FBG3 [°C]	26.2	31.2	24.9	27.9

Fig. 13 shows a picture of the result obtained for 2 W of power delivered for 150 s. At the end of the ablation, the treated area turned out to be 2 cm × 1 cm in excellent agreement with that determined by the temperature decay profile recovered from the reading of the integrated and external gratings, setting the cell necrosis temperature limit of 50 °C. The reproducibility has been tested moving the probe in other positions using the same liver; an example is test number 2 in Tab. I (corresponding to the second image from left in Fig. 14) for which we obtained similar results but with a slightly larger treated area, as testified by a slightly higher temperature read by FBG2. Longer longitudinal extensions have been obtained for the other power levels, as shown in Fig. 14. The temperature read by FBG2 in the 3 W case is lower than what expected from the analysis of the corresponding lesion size in Fig. 14 because the grating resulted to be positioned close to a blood vessel. This provides a further evidence of the necessity of redundancy in the number of gratings within the irradiated area.

The importance of carefully controlling the temperature is demonstrated in Fig. 15, where it is shown a carbonization that occurred for 4 W maintained for 150 s. Comparing the ablation parameters used for the last case in Tab. I with those that led to the carbonization (same power but different energy),

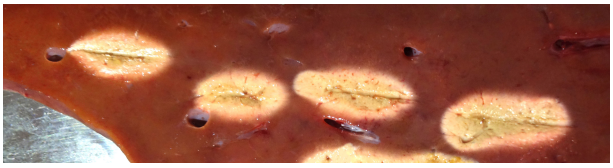

Fig. 14. Sequence of ablations keeping the energy constant at 300 J; from left to right: 2 W, repetition of 2 W, 3 W and 4 W.

Fig. 15. Example of a carbonization that occurred for 4 W of power and 150 s duration.

it is evident the key role of real time temperature monitoring to ensure proper necrosis of malignant cells while avoiding overheating.

V. Conclusion

Laser ablation is a promising treatment that presents several advantages with respect to other thermal therapies; however, its effectiveness is strictly dependent on the probe radiation pattern with respect to the tumor shape and on the induced temperature increase distribution that, in turn, to be measured in real-time requires specific sensors not influenced by the laser radiation.

To improve the LA outcomes and help increasing its clinical applications we have proposed a new optical probe based on a dual cladding optical fiber that: i) can be designed with customized irradiation pattern to fit the tissue volume to be treated; ii) embeds some FBG sensors to allow measuring in real-time the induced temperature and thus optimizing the treatment outcome.

A probe prototype designed to produce an elliptical pattern has been developed and characterized using a two-step procedure. First, with help of an ink-loaded agar gel phantom the shape of the generated thermal pattern has been evaluated from the readings of the the FBG sensors integrated in the probe combined with those of some other external FBG sensors, both validated by comparison with thermographic images. Then, further characterizations in a more realistic environment have been carried out using an ex-vivo animal liver. Some tests have been conducted for different durations and power levels, while maintaining constant the overall radiated energy. The results have shown that the thermal pattern has the same shape obtained with the agar gel phantom but the coagulated area and the temperature distribution are not only related to the radiated energy but they also depends on the presence of vessels and other tissue non-uniformities, evidencing the importance of properly monitoring the temperature to ensure reaching cytotoxic level without carbonizations. This will be even more relevant in in-vivo tests because of the presence of blood perfusion.

From the presented set of experiments it has been possible to verify that the relation between the temperature read by the gratings integrated into the probe and that of the external ones determined during ablation simulations carried out using agar phantoms and ex-vivo phantoms can be used to predict the results of real minimally invasive ablation treatments in which only the probe is inserted into the target organ.

References

[1] K.F. Chu, and D.E. Dupuy, "Thermal ablation of tumours: biological mechanisms and advances in therapy," *Nature Reviews Cancer*, Vol.14, pp. 199–208, 2014.

[2] R.J. Stafford, D. Fuentes, A.A. Elliott, J.S. Weinberg, and K. Ahrar, "Laser-induced thermal therapy for tumor ablation," *Crit Rev Biomed Eng.*, Vol. 38, pp. 79–100, 2010.

[3] T.J. Vogl, V. Freier, N.E. Nour-Eldin, K. Eichler, S. Zangos, and N.N. Naguib, "Magnetic resonance-guided laser-induced interstitial thermotherapy of breast cancer liver metastases and other noncolorectal cancer liver metastases: an analysis of prognostic factors for long-term survival and progression-free survival," *Invest Radiol.*, Vol. 48, pp. 406–412, 2013.

[4] C.L. Brace, "Radiofrequency and microwave ablation of the liver, lung, kidney, and bone: what are the differences?," *Curr. Probl. Diagn. Radiol.*, Vol. 38, pp. 135–143, 2009.

[5] M. Ahmed, C.L. Brace, F.T. Lee Jr., and S.N. Goldberg, "Principles of and advances in percutaneous ablation," *Radiology*, Vol. 258, pp. 351–369, 2011.

[6] P. Tombesi, F. Di Vece, and S. Sartori, "Laser ablation for hepatic metastases from neuroendocrine tumors," *Am. J. of Roentgenology*, Vol. 2014, paper W732, 2015.

[7] F.M. Di Matteo, M. Martino, R. Rea, et al., "US-guided application of Nd:YAG laser in porcine pancreatic tissue: an ex vivo study and numerical simulation," *Gastrointestinal Endoscopy*, Vol. 78, pp. 750-755, 2013.

[8] J.P. Ritz, K.S. Lehmann, T. Schumann, V. Knappe, U. Zurbuchen, H.J. Buhr, and C. Holmer, "Effectiveness of various thermal ablation techniques for the treatment of nodular thyroid disease–comparison of laser-induced thermotherapy and bipolar radiofrequency ablation," *Lasers Med. Sci.*, Vol. 26, pp. 545–552, 2011.

[9] P. Saccomandi, E. Schena, and S. Silvestri, "Techniques for temperature monitoring during laser-induced thermotherapy: an overview," *Int. J. of Hyperthermia*, November 2013, Vol. 29, pp. 609–619, 2013.

[10] E. Schena, P. Saccomandi, F. Giurazza, M.A. Caponero, L. Mortato, F.M. Di Matteo, F. Panzera, R. Del Vescovo, B. Beomonte Zobel and S. Silvestri, "Experimental assessment of CT-based thermometry during laser ablation of porcine pancreas," *Physics in Medicine and Biology*, Vol. 58, pp. 5705, 2013.

[11] D.A. Christensen, "Thermal dosimetry and temperature measurements," *Proc. of Conf. on Hyperthermia of Cancer Treatment*, San Diego, California, 1978.

[12] W. Chen, R. Gassino, Y. Liu, A. Carullo, G. Perrone, A. Vallan, and D. Tosi, "Performance assessment of FBG temperature sensors for laser ablation of tumors," *IEEE Int. Symp. Medical Measurements and Applications (MeMeA)*, pp.324–328, 2015.

[13] A.D. Kersey, M.A. Davis, H.J. Patrick, M. LeBlanc, K.P. Koo, C.G. Askins, M.A. Putnam, and E.J. Friebele, "Fiber grating sensors," *J. Lightwave Technol.*, Vol. 15, pp. 1442–1463, 1997.

[14] Yun-Jiang Rao, D.J. Webb, D.A. Jackson, Lin Zhang, and I. Bennion, "In-fiber Bragg-grating temperature sensor system for medical applications," *J. Lightwave Technol.*, Vol. 15, pp. 779–785, 1997.

[15] D. Tosi, E.G. Macchi, and A. Cigada, "Fiber-optic temperature and pressure sensors applied to radiofrequency thermal ablation in liver phantom: methodology and experimental measurements," *J. of Sensors*, Vol. 2015, Article ID 909012, 2015.

[16] K. de Morais Sousa, A.A. Hafner, E.G. Carati, H.J. Kalinowski, and J.C. Cardozo da Silva, "Validation of thermal and electrical model for induction motors using fiber Bragg gratings," *Measurement*, Vol. 46, pp. 1781–1790, 2013.

[17] P. Niewczas, L. Dziuda, G. Fusiek, J.R. McDonald, "Design and evaluation of a preprototype hybrid fiber-optic voltage sensor for a remotely interrogated condition monitoring system," *IEEE Trans. Instrum. Meas.*, Vol. 54, pp. 1560–1564, 2005.
[18] G. Fusiek, P. Niewczas, A. J. Willshire, and J. R. McDonald, "Nonlinearity Compensation of the Fiber Bragg Grating Interrogation System Based on an Arrayed Waveguide Grating," *IEEE Trans. Instrum. Meas.*, Vol. 57, pp. 2528–2531, 2008.
[19] S. Kannan, J.Z.Y. Guo, and P.J. Lemaire, "Thermal Stability Analysis of UV-Induced Fiber Bragg Gratings," *J. Lightwave Technol.*, Vol. 15, pp. 1560–1564, 1997.
[20] Rong-mei Liua, Da-kai Lianga, and A. Asundib, "Small diameter fiber Bragg gratings and applications," *Measurement*, Vol. 46, pp. 3440–3448, 2013.
[21] Y. Liu, W. Chen, H. Yu, R. Gassino, A. Braglia, M. Olivero, A. Vallan, and G. Perrone, "All-fiber probe for laser-induced thermotherapy with integrated temperature measurement capabilities," *Proc. SPIE*, Vol. 9317, pp.1–6, 2015.
[22] A. Braglia, A. Califano, Y. Liu, and G. Perrone, "Architectures and components for high power CW fiber lasers," *Int. J. Mod. Phys. B*, Vol. 28, pp.1–14, 2014.
[23] Y. Liu, R. Gassino, A. Braglia, A. Vallan, and G. Perrone, "Fibre probe for tumour laser thermotherapy with integrated temperature measuring capabilities," *El. Lett.*, Vol. 52, pp. 798–800, 2016.
[24] Y. Liu, R. Gassino, H. Yu, A. Braglia, A. Vallan, D. Tosi, and G. Perrone, "Improved fiber probe for laser tissue ablation with integrated distributed temperature sensor," *Proc. SPIE*, Vol. 9702, pp. 1–7, 2016.
[25] D. Tosi, S. Korganbayev, N. Zhakin, R. Gassino, G. Perrone, and A. Vallan, "Towards inline spatially resolved temperature sensing in thermal ablation with chirped fiber Bragg grating," *2016 IEEE Int. Symp. Medical Measurements and Applications (MeMeA)*, pp.1-6, 2016.
[26] X. Bao and L. Chen, "Recent Progress in Distributed Fiber Optic Sensors," *Sensors*, Vol. 12, pp. 8601–8639, 2012.
[27] K. Chen, X. Zhou, W. Peng, and Q. Yu, "OFDR based distributed temperature sensor using the three-channel simultaneous radio-frequency lock-in technique," *Photonic Sensors*, Vol. 5, pp. 217–223, 2015.
[28] W. Hill, J. Kbuler, and M. Fromme, "Single-mode distributed temperature sensing using OFDR," *Proc. SPIE*, Vol. 7653, pp. 1–5, 2010.
[29] B.J. Soller, D.K. Gifford, M.S. Wolfe, and M.E. Froggatt, "High resolution optical frequency domain reflectometry for characterization of components and assemblies," *Optics Express*, Vol. 13, pp. 666–674, 2005.
[30] C.T. Germer, A. Roggan, J.P. Ritz et al., "Optical properties of native and coagulated human liver tissue and liver tissue and liver metastases in the near infrared range," *Lasers in Surgery and Medicine*, Vol. 23, pp. 194–203, 1998.
[31] S.L. Jacques, "Optical properties of biological tissues: a review", *Phys. Med. Biol.*, Vol. 58, pp. R37–R61, 2013.
[32] J. Lim, Q. Yang, B.E. Jones, and P. R. Jackson, "Strain and temperature sensors using multimode optical fiber Bragg gratings and correlation signal processing," *IEEE Trans. Instrum. Meas.*, Vol. 51, n. 5, pp. 622–627, 2002.
[33] M. Zhang, Z. Che, J. Chen, H. Zhao, L. Yang, Z. Zhong, and J. Lu, "Experimental determination of thermal conductivity of water-agar gel at different concentrations and temperatures,
J. of Chem. and Eng. Data, Vol. 56, pp. 859–864, 2011.
[34] P.D. Ninni, F. Martelli, and G. Zaccanti, "The use of India ink in tissue-simulating phantoms", *Optics Express*, Vol. 18, pp. 26854–26865, 2010.
[35] A.Candiani, A.Bertucci, S.Giannetti, M.Konstantaki, W.Margulis, A.Manicardi, S.Pissadakis, A.Cucinotta, R.Corradini, and S.Selleri, "Label-free DNA biosensor based on a peptide nucleic acid-functionalized microstructured optical fiber Bragg grating," *J. Biomed. Opt.*, Vol. 18, paper 057004, 2013.
[36] J.A. Kaufman, M.J. Lee, "Vascular and interventional radiology: the requisites," *Elsevier Health Sciences*, 2013.